Published in final edited form as:
Sci Signal. ; 9(412): ra10. doi:10.1126/scisignal.aad7808.

Cholesterol modulates Orai1 channel function

Isabella Derler[1,*], **Isaac Jardin**[1], **Peter B. Stathopulos**[2], **Martin Muik**[1], **Marc Fahrner**[1], **Vasilina Zayats**[3], **Saurabh K. Pandey**[3], **Michael Poteser**[4], **Barbara Lackner**[1], **Marketa Absolonova**[1], **Rainer Schindl**[1], **Klaus Groschner**[4], **Rüdiger Ettrich**[3], **Mitsu Ikura**[5], and **Christoph Romanin**[1,*]

[1]Institute of Biophysics, Johannes Kepler University of Linz, Gruberstrasse 40, 4020 Linz, Austria

[2]Department of Physiology and Pharmacology, Schulich School of Medicine and Dentistry, University of Western Ontario, London, Ontario N6A 5C1, Canada

[3]Center for Nanobiology and Structural Biology, Institute of Microbiology, Academy of Sciences of the Czech Republic, CZ-373 33 Nové Hrady, Czech Republic

[4]Institute of Biophysics, Medical University of Graz, Harrachgasse 21/4, 8010 Graz, Austria

[5]Princess Margaret Cancer Centre and Department of Medical Biophysics, University of Toronto, Toronto, Ontario M5G 1L7, Canada

Abstract

STIM1 (stromal interaction molecule 1) and Orai proteins are the essential components of Ca^{2+} release–activated Ca^{2+} (CRAC) channels. We focused on the role of cholesterol in the regulation of STIM1-mediated Orai1 currents. Chemically induced cholesterol depletion enhanced store-operated Ca^{2+} entry (SOCE) and Orai1 currents. Furthermore, cholesterol depletion in mucosal-type mast cells augmented endogenous CRAC currents, which were associated with increased degranulation, a process that requires calcium influx. Single point mutations in the Orai1 amino terminus that would be expected to abolish cholesterol binding enhanced SOCE to a similar extent as did cholesterol depletion. The increase in Orai1 activity in cell expressing these cholesterol-binding–deficient mutants occurred without affecting the amount in the plasma membrane or the coupling of STIM1 to Orai1. We detected cholesterol binding to an Orai1 amino-terminal fragment in vitro and to full-length Orai1 in cells. Thus, our data showed that Orai1 senses the amount of cholesterol in the plasma membrane and that the interaction of Orai1 with cholesterol inhibits its activity, thereby limiting SOCE.

Introduction

Precise control of Ca^{2+} homeostasis and signaling is indispensible for various cellular processes (1). Store-operated calcium channels (SOCs) represent the main Ca^{2+} entry

[*]Corresponding author. isabella.derler@jku.at (I.D.); christoph.romanin@jku.at (C.R.).

Author contributions: I.D. and C.R. conceived the project, designed the experiments, and wrote the manuscript. I.D., I.J., P.B.S., M.M., M.F., V.Z., S.K.P., M.P., B.L., and M.A. performed the experiments and analyzed the data. R.S., P.B.S., R.E., M.I., and K.G. helped write the manuscript and were involved in data discussions.

Competing interests: The authors declare that they have no competing interests.

Europe PMC Funders Author Manuscripts

pathway into the cell, among which the Ca^{2+} release–activated Ca^{2+} (CRAC) channel is best characterized (2, 3). The molecular key components of the CRAC channel are the endoplasmic reticulum (ER)–located Ca^{2+}-sensing stromal interaction molecule 1 (STIM1) (4, 5) and the pore-forming subunit of the CRAC channel, termed Orai1 (6–8). Upon depletion of ER Ca^{2+}, STIM1 multimerizes and redistributes into discrete puncta at plasma membrane–ER junctions (9, 10). Subsequently, it couples to and stimulates Orai1, initiating CRAC currents (11). There are three Orai homologs, termed Orai1 to Orai3 (7), which all contain four transmembrane (TM) segments and cytosolic N and C termini and form tetrameric or hexameric Orai subunit assemblies, which are Ca^{2+}-selective plasma membrane channels (12, 13). STIM1 couples to the Orai1 C terminus (11, 14), and coupling and gating involve the extended TM Orai1 N-terminal (ETON) region in the Orai1 N terminus, which forms a helical extension of TM1 into the cytosol (13, 15). The latter STIM1-Orai1 interaction, which involves hydrophobic as well as positively charged residues, occurs with a weak affinity in the micromolar range (15). Moreover, two pore-lining positively charged residues in the ETON region and Arg^{91} contribute to the Orai1 gate by electrostatic stabilization and by forming a barrier to the pore in the closed Orai1 conformation (16). Point mutation of Arg^{91} to a hydrophobic tryptophan results in complete loss of function, which is responsible for a form of severe combined immunodeficiency syndrome (6, 17), and which occurs because of an increased hydrophobicity at the N terminus/TM interface (18). Although STIM1 and Orai are sufficient to fully reconstitute CRAC currents, other various proteins have already been suggested to regulate STIM1 and Orai function (19–23). Not only proteins but also lipids such as phosphatidylinositol 4,5-bisphosphate can regulate SOC entry (24–26).

Here, we reported on a regulatory role of cholesterol in store-operated Orai1 currents. Cholesterol depletion led to an increase in Orai1-mediated currents in human embryonic kidney (HEK) cells and in endogenous CRAC currents in mast cells. In support of these findings, we detected cholesterol association with Orai1, and point mutations within Orai1 that impaired cholesterol association enhanced currents in a similar manner to cholesterol depletion. Hence, we propose that cholesterol modulates CRAC channel function.

Results

Cholesterol-depleting agents increase STIM1-mediated Orai1 currents

To characterize the modulatory impact of cholesterol on Orai1 function, we used cholesterol oxidase and filipin to deplete and segregate cholesterol. Cholesterol oxidase is an enzyme that induces chemical derivatization of plasma membrane cholesterol to cholestenone (27), and filipin binds to cholesterol, generating filipin-cholesterol complexes, which disrupt the integrity of sterol-containing membranes (28). After pretreatment with cholesterol oxidase, fluorescent Ca^{2+} imaging revealed significantly enhanced thapsigargin (TG)–induced Ca^{2+} entry in STIM1- and Orai1-containing HEK293 cells (Fig. 1A). Correspondingly, we recorded an about twofold increase in CRAC currents, evoked upon passive store depletion in the whole-cell patch-clamp configuration (Fig. 1B). Inactivation and reactivation characteristics of STIM1-mediated Orai1 currents during a voltage step to −90 mV remained unaffected upon incubation with cholesterol oxidase (Fig. 1C). Similar to cholesterol

oxidase treatment, preincubation with filipin resulted in enhanced STIM1-Orai1–mediated Ca^{2+} entry (Fig. 1D) and increased Ca^{2+} currents (Fig. 1E). The augmented Ca^{2+} influx did not arise from increased Orai1 abundance in the plasma membrane, as determined from fluorescence intensities (Fig. 1F) and cell surface biotinylation assays (Fig. 1G), or enhanced STIM1-Orai1 overall interaction, as revealed by coimmunoprecipitation (Fig. 1H), in the presence or absence of cholesterol oxidase. Thus, these results obtained with STIM1- and Orai1-expressing HEK cells pointed to a modulatory role of cholesterol in Orai1 channel function.

Cholesterol depletion enhances endogenous CRAC currents and mast cell degranulation in RBL cells

To recapitulate the cholesterol effect with endogenous CRAC currents of mast cells, we investigated the functional role of cholesterol in mucosal-type rat basophilic leukemia (RBL) 2H3 cells through responses to chemically induced cholesterol depletion. Ca^{2+} imaging revealed that pretreatment with cholesterol oxidase significantly enhanced TG-induced Ca^{2+} entry of RBL cells (Fig. 1I). Analogously, we recorded a significant increase in store-operated Ca^{2+} currents upon passive store depletion using the patch-clamp technique (Fig. 1J). Furthermore, hexosaminidase release, a marker of degranulation (29), was enhanced in cholesterol-depleted cells compared to control RBL cells (Fig. 1K). This effect might be of pathophysiological relevance because increased degranulation is a feature of mast cells from patients with Smith-Lemli-Opitz syndrome (SLOS), a type of hypocholesterolemia (30). Together, these results suggested that cholesterol depletion induced increased Ca^{2+} entry through endogenous Orai1 channels, thus leading to increased degranulation in RBL mast cells.

Mutations in the Orai1 ETON region enhance Ca^{2+} entry and Ca^{2+} currents

On the basis of the similar effects of cholesterol depletion on reconstituted and endogenous CRAC currents, we sought to identify a putative cholesterol binding site in the primary sequence of Orai1. Indeed, we identified the so-called cholesterol recognition/interaction amino acid consensus motif [cholesterol-binding (CB) motif] (31) in the ETON region, which interacts with STIM1 (14, 32), CaM (33, 34), and CRACR2A (35). Within this ETON region, a segment encompassing residues 74 to 83 (LSWRKLYLSR) matches the cholesterol binding consensus motif-[L/V]-$(X)_{1–5}$-Y-$(X)_{1–5}$-[K/R]- (fig. S1) (31). To test whether this region was required for the effect of cholesterol on Orai1, we introduced single point mutations within the potential CB motif similar to those that successfully reduce the sequestration of cholesterol with other proteins (31, 36). Substitutions of L → I and Y → S (31, 36) have emerged as most effective in disrupting the function of the CB motif. Thus, we initially substituted Ile for Leu^{74} (Orai1 L74I) or Ser for Tyr^{80} (Orai1 Y80S). We separately analyzed these Orai1 mutants cotransfected with STIM1 in HEK293 cells by Ca^{2+} imaging and patch clamping. After application of TG, the Orai1 L74I or Orai1 Y80S mutant exhibited significantly enhanced Ca^{2+} entry (Fig. 2, A and B), when compared to the wild-type form. Consistently, electrophysiological recordings yielded nearly doubled store-operated currents with Orai1 L74I or Orai1 Y80S in comparison to wild-type Orai1 (Fig. 2, C and D). Analogously, when stimulated by the Orai-activating small fragment (OASF; STIM1 amino acids 233 to 474) (37), these Orai1 mutants exhibited about a twofold

increase in currents compared to wild-type Orai1 (Fig. 2E). Because of unknown reasons, the increased Ca^{2+} entry and the currents consistently observed with the Orai1 Y80S mutant are at variance with the report of Mullins *et al.* (34) who found current densities similar to wild-type Orai1. Nonetheless, increased currents did not arise from enhanced plasma membrane targeting, as evidenced by comparable plasma membrane fluorescence intensities for the Orai1 L74I or Y80S mutants and wild-type Orai1 (Fig. 2F). Moreover, cell surface biotinylation experiments revealed a comparable amount of protein in the plasma membrane for both the mutants and wild-type Orai1 (Fig. 2G).

Further, we used confocal Förster resonance energy transfer (FRET) microscopy to investigate the interaction of OASF (amino acids 233 to 474) with the Orai1 mutants and the wild-type form. FRET between OASF and the Orai1 L74I or Y80S mutant was similar to wild-type Orai1 (Fig. 2H). Normalized intensity profiles of OASF from cells containing either wild-type Orai1 or the Orai1 L74I mutant in the plasma membrane were comparable and did not show an altered association (fig. S2A). TG induced similar increases in FRET with similar maximum values between STIM1 and Orai1 L74I or wild-type Orai1 (fig. S2B), suggesting that increased currents did not arise from faster or enhanced overall STIM1-Orai1 coupling. Because STIM1 binding occurs mainly at the Orai1 C terminus and only to a weaker extent at the Orai1 N terminus (14, 15), an altered interaction of STIM1 with the Orai1 N terminus cannot be excluded, but probably cannot be detected by FRET. Thus, L74I or Y80S mutation within the putative CB motif in Orai1 resulted in strongly increased Ca^{2+} entry and currents (Fig. 2, A to D), without significantly affecting the amount of Orai1 protein in the plasma membrane and overall coupling to STIM1.

The Orai1 L74I and Y80S mutants are insensitive to cholesterol depletion

If L74I and Y80S mutations interfere with the ability of Orai1 to respond to cholesterol, the cholesterol depletion agents should have no further effect on Ca^{2+} entry or CRAC currents. Indeed, Ca^{2+}-imaging measurements revealed no further increase in Ca^{2+} entry upon pretreatment with cholesterol oxidase or filipin from cells cotransfected with STIM1 and either the L74I or Y80S mutant (Fig. 3, A and B, and fig. S3), in contrast to the stimulated Ca^{2+} entry of the wild-type proteins. Concordantly, electrophysiological recordings of HEK293 cells cotransfected with STIM1 and the Orai1 L74I or Orai1 Y80S mutant before and after pretreatment with cholesterol oxidase demonstrated no significant difference in store-operated currents activated upon passive store depletion (Fig. 3, C and D). Furthermore, the amount of Orai1 L74I and Orai1 Y80S mutants in the plasma membrane remained comparable without and with cholesterol oxidase treatment (only shown for Orai1 L74I) as evaluated by cell surface biotinylation experiments (Fig. 3E) and plasma membrane fluorescence intensities (Fig. 3F). Together, these experiments further support the concept that cholesterol reduces Orai1 channel activity by a mechanism that is disrupted with the L74I or Y80S mutation in the ETON region.

Reloading of plasma membrane cholesterol reverses the effect of cholesterol oxidase

To further support the cholesterol effect on Orai1 channels, we performed experiments on the reversal of the cholesterol oxidase effect by reloading the cell with cholesterol using the methyl-β-cyclodextrin (MβCD)–cholesterol complex (38). We would like to note that

MβCD-cholesterol treatment of cells to replenish cholesterol was better tolerated than MβCD treatment for cholesterol depletion, which, in our hands, led to increased cell deterioration. We found that cholesterol replenishment reduced the current density produced by cells pretreated with cholesterol oxidase (Fig. 3G). In contrast, the increased currents from Orai1 L74I and Y80S mutants remained unaffected by additional cholesterol loading (Fig. 3, H and I), compatible with impaired cholesterol binding to these mutants. The reversal of the cholesterol oxidase–induced increase in Orai1 currents upon cell replenishment with cholesterol supports the concept of a reversible response of Orai1 channel function to cholesterol.

An Orai1 N-terminal peptide displays in vitro binding of cholesterol

We performed intrinsic fluorescence–binding studies to assess whether cholesterol bound to the ETON region–containing N terminus. For these in vitro experiments, we used a synthetic peptide including the amino acids 72 to 90 of the Orai1 N terminus, which encompasses the whole ETON region, and monitored the change of the intrinsic Trp^{76} fluorescence in the presence and absence of cholesterol. The free Orai1 N terminus exhibited an emission maximum at ~350 nm using an excitation wavelength of 280 nm. The presence of cholesterol resulted in an increase in the tryptophan fluorescence at 350 nm (Fig. 4A), suggesting in vitro cholesterol binding to the Orai1 N-terminal peptide (39). Titration of the peptide with increasing concentrations of cholesterol yielded a saturable concentration-dependent increase in fluorescence. The increase in fluorescence intensity was fitted to an equation for a single binding site with an apparent equilibrium dissociation constant (K_d) of 1.2 μM (Fig. 4B). Next, we tested the ability of L74I or Y80S mutant peptides to bind cholesterol. Both mutations weakened the affinity for cholesterol as evidenced by about an order of magnitude increase in apparent K_d values (L74I: >14 μM and Y80S: >23 μM) (Fig. 4B). Overall, these binding data suggested that the in vitro mutant peptide–cholesterol interactions were more than 11- to 18-fold weaker compared to wild type.

Additionally, we evaluated the far-ultraviolet circular dichroism (CD) spectrum of the Orai1 N-terminal peptide to experimentally assess the secondary structure of this region in solution. The CD spectrum of our peptide showed a minimum at ~222 nm, consistent with the formation of α-helix; however, the more intense minimum at ~203 nm suggested the presence of a large fraction of random coil (fig. S4). Hence, the peptide in solution did not adapt the strong α-helicity of this N-terminal portion in full-length Orai1 as found in the crystal structure of the assumedly closed *Drosophila* Orai (dOrai) channel (13).

In summary, our data revealed in vitro cholesterol binding to the Orai1 N-terminal peptide with an impairment of the cholesterol binding by single point mutations in the N terminus. However, because of the substantially reduced α-helicity of the Orai1 N-terminal peptide as observed by CD spectra, it remains unclear whether cholesterol binding occurs analogously in the full-length Orai1 channel. Hence, we next examined the binding of cholesterol to full-length Orai1 using FRET measurements in HEK293 cells.

Association of cholesterol with the full-length Orai1 channel is reduced by the L74I or Y80S mutation

To investigate a potential association of cholesterol to full-length Orai1 in cells, we used FRET–total internal reflection fluorescence (FRET-TIRF) microscopy. For these in vivo experiments, we used TopFluor Cholesterol (40) and HEK293 cells containing Cherry-STIM1 and cyan fluorescent protein (CFP)–Orai1. Before and after store depletion by TG, TIRF imaging revealed substantial FRET between CFP-Orai1 and TopFluor Cholesterol (Fig. 4, C to E). In contrast, FRET-TIRF from HEK cells containing the L74I or Y80S mutant was markedly reduced, both before and after store depletion (Fig. 4, C to E). Thus, these results suggested the close proximity of full-length Orai1 to cholesterol independently of store depletion, and reduced coupling of the L74I and Y80S mutants to cholesterol.

Discussion

The present study uncovered a regulatory role of cholesterol in CRAC channel function. The reduction in the amount of cholesterol by various means resulted in an increase in Ca^{2+} entry and currents from HEK cells expressing Orai1 channels. Endogenous CRAC currents of RBL mast cells were similarly increased upon cholesterol depletion, leading to enhanced mast cell degranulation. Cholesterol association with the full-length Orai1 channel complex was reduced by L74I and Y80S mutations in the Orai1 N terminus.

Cholesterol is mainly enriched in lipid raft domains, which are detergent-resistant plasma membrane microdomains (41). Orai1, STIM1, and TRP (transient receptor potential) members such as TRPC1 (TRP channel 1), TRPC4, and TRPC5 have been reported to localize to lipid rafts. Loss of cholesterol alters their localization or association (42–44) in line with the potential impact of lipid raft domains and cholesterol on STIM1 and Orai signaling. Moreover, Orai1 has been found in lipid rafts in close proximity to potassium channels in breast and prostate cancer cells (45).

Our FRET measurements of full-length Orai1 suggested that cholesterol was associated with the Orai1 channel complex, the interaction of which was affected by mutations within the ETON region. These mutations (L74I or Y80S), which were designed to target a potential CB motif in the ETON region in accordance with other studies (31), increased Orai1 channel activity to a similar value as induced by cholesterol depletion. Cholesterol bound to an N-terminal Orai1 peptide including the ETON region in vitro. In vitro CD spectra showed that the N-terminal peptide contained a mixture of α-helix and random coil in solution, contrary to what is seen in the dOrai crystal structure. These data imply that α-helicity may not be obligatory for cholesterol binding to the Orai1 N terminus, as has been suggested for other peptide or protein segments (31, 46–48). The dOrai crystal structure, which is presumed to be of the closed channel, shows the Leu^{74} and Tyr^{80} residues localized on opposite sides of a fully a-helical ETON region. Thus, an unstructuring of the ETON helix would be required for both Leu^{74} and Tyr^{80} to simultaneously contribute to cholesterol binding. Along the same lines, the elongated TM1 segments, which are physically distant from the membrane, are surrounded by a large body of other, adjacent TM helices in the dOrai crystal structure, rendering an interaction between the putative CB motif in the N-terminal extension of TM1 and cholesterol difficult without any conformational reorientation. Nevertheless, FRET

measurements suggested diminished coupling of cholesterol to the L74I and Y80S mutants compared to wild-type Orai1 in live cells, which is compatible both with a direct effect of the L74I and Y80S mutations on cholesterol association in the full-length Orai1 channel complex and with the possibility that other potential cholesterol binding sites within Orai1 are negatively affected in an allosteric manner upon these N-terminal mutations.

Cholesterol has been reported to regulate the ion channel function of TRPV1 and Kir2 (49, 50). In both channels, cholesterol has been suggested to affect the open conformations. Because the basic region of the TM1 helix has been suggested to have some gating function (13, 15), it is tempting to speculate that cholesterol might reduce flexibility at the ETON region, thereby attenuating Ca^{2+} entry. The positioning of the Orai1 helices for both the closed- and open-channel conformations in a genuine membrane environment is currently unknown. The varying of membrane thickness in the presence and absence of cholesterol (about 2 to 3 Å) can regulate protein function (51, 52) because of the adaption of TM helices to membrane thickness (53, 54). Hence, we cannot rule out that the cholesterol content in the plasma membrane might have an additional, indirect regulatory impact on the maximal activation of Orai1 channels because of the modulation of membrane thickness.

The cholesterol effect on Orai1 channel function was reversible upon cholesterol reloading of cells previously treated with cholesterol-depleting agents. Although cholesterol depletion by MßCD has been previously shown to reduce, rather than increase, CRAC entry (42, 55), MßCD removes cholesterol from the membrane (42), whereas cholesterol oxidase transforms cholesterol to cholestenone, and it is unknown whether cholestenone stays in the membrane (27). Further, we and others (27, 56) observed increased cell deterioration after incubation with MßCD, which was why we preferred the less harsh treatment of cells with cholesterol oxidase and filipin.

Cholesterol has also been reported to play a role in the immune system. Individuals with SLOS, a type of hypocholesterolemia, cannot produce cholesterol, accumulate 7-dehydrocholesterol in lipid rafts, and suffer from immune system defects such as allergies (30). Further, degranulation of mast cells that cannot take up cholesterol is significantly increased compared to wild-type cells (30). We observed in this study a similar phenomenon for cholesterol-depleted RBL mast cells, which showed an increase in both CRAC currents and degranulation. Here, our data additionally suggest a mechanistic link between cholesterol depletion and Orai1 function.

In summary, we have demonstrated that Orai1 channels are regulated by cholesterol, which suppresses CRAC channels. Mutations in the putative CB motif in the Orai1 N terminus antagonized the cholesterol effect, suggesting that this region plays a role in channel regulation, in either a direct or allosteric manner. A high-resolution structure of an Orai1-cholesterol complex is needed to understand the precise structural determinants of the interaction and the effect on the gating.

Materials and Methods

Molecular cloning and mutagenesis

Human Orai1 (Orai1; accession no. NM_032790) was provided by A. Rao's Laboratory, Harvard Medical School. N-terminally tagged Orai1 constructs were cloned with Sal I and Sma I restriction sites of pECFP-C1 and pEYFP-C1 expression vectors (Clontech). pEYFP-Orai1 served as template for the generation of pEYFP–Orai1 L74I and pEYFP–Orai1 Y80S. All mutants were constructed with the QuikChange Site-Directed Mutagenesis Kit (Stratagene). The integrity of all resulting clones was confirmed by sequence analysis. Human STIM1 (STIM1; accession no. NM_003156) N-terminally tagged with enhanced CFP (ECFP) and enhanced yellow fluorescent protein (EYFP) was provided by T. Meyer's Laboratory, Stanford University.

Cholesterol depletion and replenishment

Depletion of cellular cholesterol was induced by application of either cholesterol oxidase (Sigma-Aldrich Handels GmbH, product no. C8649) or filipin (Sigma-Aldrich Handels GmbH, product no. F9765). For preparing the stock solution, filipin was initially reconstituted in anhydrous dimethyl sulfoxide (C_2H_6OS, Merck Chemicals International, product no. 1029311000) at 1 μg/ml and was then diluted in buffer without Ca^{2+} to yield an end concentration of 1 μg/ml, which was incubated for 60 min at 37°C. Cholesterol oxidase was solubilized in H_2O to obtain a stock solution of 20 U/ml and was further diluted in Ca^{2+}-free buffer to receive an end concentration of 2 U/ml, which was incubated for 20 min at 37°C.

For replenishment of cellular cholesterol, complexes of cholesterol and MβCD (Sigma-Aldrich) were prepared by a modification of a previously described protocol (38). Briefly, 10 ml of an aqueous solution of MβCD (45 mM) and 300 μl of isopropyl alcohol containing 0.018 g of cholesterol were heated to 80°C. Afterward, the cholesterol solution was added dropwise with stirring into the MβCD solution. After dispersal of cholesterol, the solution was allowed to cool at room temperature. Aliquots (5 ml) of the solution were placed in 50-ml centrifuge tubes, frozen with liquid nitrogen, and lyophilized. The lyophilized MβCD-cholesterol complexes were stored at −20°C. Each aliquot was dissolved in 22.5 ml of buffer to obtain a final concentration of 10 mM before experiments.

Cell culture and transfection

Transient transfection of HEK293 cells was performed using either the TransFectin Lipid Reagent (Bio-Rad) or the TransPass Transfection Reagent (New England BioLabs).

Ca^{2+} imaging using the fluorescent dye fura-2 AM

HEK293 cells were transfected (TransFectin, Bio-Rad) with 0.7 μg of mCherry-STIM1 and 0.7 μg of DNA of YFP-Orai1 constructs and mutants. RBL cells were not transfected. Twenty- to 24-hour transfected HEK293 or nontransfected RBL cells were loaded with 2 μM fura-2 AM (acetoxymethyl ester) (Sigma-Aldrich, production no. F0888) for 20 min at 37°C in a standard Ca^{2+}-free extracellular solution (140 mM NaCl, 5 mM KCl, 1 mM $MgCl_2$, 10 mM Hepes, and 10 mM glucose). The cells were then washed three times, and

dyes were allowed to deesterify for 15 min at 20°C. Coverslips were mounted on an inverted Axiovert 135 TV microscope, and fluorescence was recorded from individual cells, with excitation wavelengths of 340 and 380 nm and emission at 505 nm. Changes in intracellular Ca^{2+} concentrations were monitored using the fura-2 AM 340/380 fluorescence ratio and calibrated according to a previously established method (57). The standard extracellular solutions consisted of 145 mM NaCl, 5 mM CsCl, 1 mM $MgCl_2$, 10 mM Hepes, 10 mM glucose, and 0 or 2 mM $CaCl_2$ (pH 7.4). Regarding controls to cholesterol oxidase and filipin treatments, control cells were also preincubated at 37°C for 20 min in the extracellular Ca^{2+}-free solution. Experiments of control cells compared to treated or transfected cells were carried out in paired comparison on the same day, with a daily comparison performed for either set of experiments: STIM1 + Orai1 or Orai1 L74I or Orai1 Y80S ± cholesterol oxidase or STIM1 + Orai1 or Orai1 L74I or Orai1 Y80S ± filipin. Control experiments were also performed without and with heat-inactivated cholesterol oxidase, leading to equivalent results.

Electrophysiology

Electrophysiological experiments were performed at 21° to 25°C, using the patch-clamp technique in whole-cell recording configurations. An Ag/AgCl electrode was used as a reference electrode. For STIM1- and Orai1-mediated currents, voltage ramps were applied every 5 s from a holding potential of 0 mV, covering a range of −90 to 90 mV for 1 s. Upon maximum activation, voltage steps of −90, −70, −50, and −30 mV for 2 s were applied every 5 s from a holding potential of 0 mV. The internal pipette solution designed for passive store depletion of Orai-derived currents contained 145 mM cesium methanesulfonate, 8 mM NaCl, 3.5 mM $MgCl_2$, 10 mM Hepes, and 20 mM EGTA pH 7.2). The standard extracellular solution consisted of 145 mM NaCl, 5 mM CsCl, 1 mM $MgCl_2$, 10 mM Hepes, 10 mM glucose, and 10 mM $CaCl_2$ (pH 7.4). All currents were leak-corrected by subtracting either the initial voltage ramps obtained shortly after break-in with no visible current activation or the remaining currents after 10 μM La^{3+} application at the end of the experiment, with both yielding identical results. Experiments of control cells compared to treated or transfected cells were carried out in paired comparison on the same day.

Cholesterol binding by intrinsic Orai1 fluorescence

Intrinsic Tyr or Trp fluorescence measurements were made on a Shimadzu RF-5301PC fluorometer (Shimadzu Corp.) using an excitation wavelength of 280 nm. Samples contained 2.5 μM peptide and increasing concentrations of cholesterol [(3β)-cholest-5-en-3-ol; 0.5 to 50 μM]. Synthesized Orai1 N-terminal peptides (QALSWRKLYLSRAKLKASS) were ordered from GenScript and solubilized in a buffer containing 20 mM tris, 150 mM NaCl, 2 mM dithiothreitol, and 2% (v/v) ethanol (EtOH) (pH 8.5). Samples contained a final concentration of 2% (v/v) EtOH for cholesterol solubility. The fluorometer was temperature-equilibrated at 20°C, and data were collected in 1-ml (l = 1 cm) quartz cuvettes with the excitation and emission slit widths adjusted such that fluorescence was within the linear response range for the instrument. All measurements were corrected for cholesterol and buffer contributions using control samples in the absence of peptide. Measurements were carried out three times for each peptide.

CD spectrometry

Data were acquired in 1-nm increments on a Jasco J-815 CD spectrometer using a quartz cuvette of 0.1-cm path length at 4°C. The wavelength scan rate was 20 nm/min with a response time of 8 s and the bandwidth set at 1 nm. Experiments were acquired using protein samples at 0.275 mg/ml.

Confocal FRET fluorescence microscopy

Confocal FRET microscopy was performed as in (58). In brief, a QLC100 Real-Time Confocal System (VisiTech Int.) was used for recording fluorescence images connected to two Photometrics CoolSNAP HQ monochrome cameras (Roper Scientific) and a dual-port adapter (dichroic, 505LP; cyan emission filter, 485/30; yellow emission filter, 535/50; Chroma Technology Corp.). This system was attached to an Axiovert 200M microscope (Zeiss) in conjunction with an argon-ion multiwavelength (457, 488, and 514 nm) laser (Spectra-Physics). The wavelengths were selected by an Acousto-Optical Tunable Filter (VisiTech Int.). MetaMorph 5.0 software (Universal Imaging Corp.) was used to acquire images and to control the confocal system. Illumination times of about 900 to1500 ms were typically used for CFP, FRET, and YFP images that were consecutively recorded with a minimized delay. Before the calculation, the images had to be corrected because of crosstalk and cross-excitation, and the appropriate crosstalk calibration factors were determined for each of the constructs on the day the FRET experiments were performed. The corrected FRET image (N_{FRET}) was calculated on a pixel to pixel basis after background subtraction and threshold determination using a custom-made software (59) integrated in MATLAB 7.0.4 according to the method published in (60). The analysis was limited to pixels with a CFP/YFP molar ratio between 1:10 and 10:1 to yield reliable results (61). Plasma membrane fluorescence intensities were obtained from an area of about 2-μm length across the plasma membrane of the respective cells and calculated as the mean fluorescence intensity of all pixels (62).

FRET for TopFluor Cholesterol–CFP-Orai protein

HEK293 cells transfected with CFP-Orai1 (or mutants Orai1 L74I or Orai1 Y80S) and mCherry-STIM1 were grown in 30-mm glass bottom dishes for 2 days. Transfected cells were loaded with 2.5 μM TopFluor Cholesterol (Avanti Polar Lipids; excitation/emission, 495/507 nm] for 2 hours in culture medium. Before the experiment, the loading medium was replaced by nominally Ca^{2+}-free buffer. After 5 min in Ca^{2+}-free buffer, stores were depleted by the addition of 2 μM TG (Sigma-Aldrich), and images were recorded after a further 5 min.

An Orca-D2 (Hamamatsu Photonics) split-view camera was used for separating FRET images and was attached to an Observer D1 microscope (Zeiss) in conjunction with a 455/488/561-nm Laser System (Visitron Systems GmbH). VisiVIEW imaging software (Visitron Systems) was used to record images. Images were analyzed using ImageJ (W. S. Rasband, U.S. National Institutes of Health, 1997 to 2014, http://imagej.nih.gov/ij/).

For correction of the FRET channel image bleedthrough, the corrected FRET image (nFRET) was calculated after background subtraction using the sensitized emission

correction method: nFRET = rawFRET − corrD * $I_{donator}$ − corrA * $I_{acceptor}$. The calibration parameters were obtained from experiments using HEK cells containing only Orai1-CFP or nontransfected HEK cells loaded with TopFluor Cholesterol (corrD = 0.83, corrA = 0.14). FRET pixel intensities were then corrected for colocalization with the ImageJ FRET analyzer plugin and expressed in relation to donor and acceptor intensities (nFRET). To obtain comparable values between cells, a cell nFRET was calculated by normalizing mean nFRET to the percentage of nFRET-positive pixels in the basolateral surface area of each cell.

Degranulation of mucosal-type mast cells

RBL 2H3 cells were grown in 24-well plates overnight in a 37°C incubator. Upon removal of the medium and washing, the cells were incubated in 2 mM Ca^{2+} solution containing bovine serum albumin for 5 min. Store depletion was induced by 200 nM TG, and 100-μl aliquots were taken at 10, 15, 20, and 30 min. Control aliquots were also taken from cells in the resting state and from cells displaying full degranulation upon incubation in a 2% (v/v) Triton X-100 solution. Then, 200 μl of a solution containing 1.3 mg of *p*-nitrophenyl-*N*-acetyl-β-D-glucosamine in 1 ml of 0.1 M sodium citrate solution (pH 4.5) was added and incubated for 1 hour. The reaction was stopped with 600 μl of 0.2 M glycine solution. The extent of degranulation was assessed by the absorbance of the samples at 405 nm. The percentage degranulation was calculated by subtracting the basal degranulation from that obtained after store depletion and then normalized to the maximal degranulation.

Biotinylation of cell surface membrane proteins

EZ-Link Sulfo-NHS-LC-biotin and High Capacity Streptavidin Agarose Resin were purchased from Pierce; anti-Orai1 and anti–β-actin antibodies were from Sigma-Aldrich; peroxidase-linked anti-rabbit IgG (immunoglobulin G) was from Amersham. Cell biotinylation was performed as described previously (63). Briefly, HEK293 cells were transfected with wild-type YFP-Orai1 or different YFP-Orai1 mutants. After 24 to 72 hours, cell surface proteins were incubated for 1 hour at 4°C using EZ-Link Sulfo-NHS-LC-biotin (0.5 mg/ml; Pierce). After incubation, 100 mM tris was added to stop the reaction. Cells were washed twice with phosphate-buffered saline (PBS) to remove excess biotinylation agent and then lysed with lysis buffer (pH 8.0) containing 100 mM NaCl, 20 mM tris, 2 mM EDTA, 10% glycerol, and 0.5% NP-40 and supplemented with Protease Inhibitor Cocktail (20 μl/ml; Roche Applied Science). Lysed samples were centrifuged at 14,000*g* for 15 min. Finally, biotinylated proteins in the supernatant were precipitated using High Capacity Streptavidin Agarose Resin (Pierce) overnight at 4°C on a rocking platform. The samples were resolved by 12% SDS–polyacrylamide gel electrophoresis, and protein detection was done using the antibody against Orai1 diluted 1:2000 in PBS– Tween 20 (PBST). The primary antibody was removed, and blots were washed six times for 5 min each with PBST. To detect the primary antibody, blots were incubated for 1 hour with horseradish peroxidase–conjugated rabbit anti-mouse IgG antibody diluted 1:5000 in PBST and then exposed to enhanced chemiluminescence reagents for 2 min. Blots were then exposed to photographic films. The density of bands on the film was measured using scanning densitometry. The amount of Orai1 in the whole protein input was used to normalize the amount of protein.

Immunoprecipitation and immunoblotting

Immunoprecipitation and Western blotting were performed as described previously (63). In brief, 500-μl aliquots of HEK293 suspension (2×10^5 cells/ml) were lysed with an equal volume of lysis buffer (pH 8.0) containing 200 mM NaCl, 40 mM tris, 4 mM EDTA, 20% glycerol, and 1% NP-40 and supplemented with Protease Inhibitor Cocktail (20 μl/ml; Roche Applied Science). Aliquots of HEK293 lysates (1 ml) were immuno-precipitated by incubation with 1 μg of either an STIM1-recognizing antibody (BD Biosciences) or an Orai1-recognizing antibody (Sigma-Aldrich) (64) and 25 μl of protein A–agarose overnight at 4°C on a rocking platform. The immunoprecipitates were resolved as described above. Data were normalized to the amount of protein recovered by the antibody used for the immunoprecipitation (65).

Supplementary Materials

Refer to Web version on PubMed Central for supplementary material.

Acknowledgments

We thank S. Buchegger for excellent technical assistance. Human Orai1 was provided by A. Rao (Harvard Medical School). Human STIM1 N-terminally tagged with eCFP and eYFP was provided by T. Meyer (Stanford University). **Funding:** This work was supported by the Austrian Science Fund (FWF projects P25210 and P27641 to I.D., FWF project M01506000 to I.J., FWF projects P26067 and P28701 to R.S., and FWF projects P25172 and P27263 to C.R.) and grant support from the Canadian Institutes for Health Research and Heart and Stroke Foundation of Canada (to M.I.). M.I. holds the Canada Research Chair in Cancer Structural Biology. R.E. acknowledges support from the Czech Science Foundation (13-21053S).

References and Notes

1. Berridge MJ, Bootman MD, Roderick HL. Calcium signalling: Dynamics, homeostasis and remodelling. Nat Rev Mol Cell Biol. 2003; 4:517–529. [PubMed: 12838335]
2. Zweifach A, Lewis RS. Mitogen-regulated Ca2+ current of T lymphocytes is activated by depletion of intracellular Ca2+ stores. Proc Natl Acad Sci U S A. 1993; 90:6295–6299. [PubMed: 8392195]
3. Lewis RS. Store-operated calcium channels. Adv Second Messenger Phosphoprotein Res. 1999; 33:279–307. [PubMed: 10218123]
4. Liou J, Kim ML, Heo WD, Jones JT, Myers JW, Ferrell JE Jr, Meyer T. STIM is a Ca^{2+} sensor essential for Ca^{2+}-store-depletion-triggered Ca^{2+} influx. Curr Biol. 2005; 15:1235–1241. [PubMed: 16005298]
5. Zhang SL, Yu Y, Roos J, Kozak JA, Deerinck TJ, Ellisman MH, Stauderman KA, Cahalan MD. STIM1 is a Ca^{2+} sensor that activates CRAC channels and migrates from the Ca^{2+} store to the plasma membrane. Nature. 2005; 437:902–905. [PubMed: 16208375]
6. Feske S, Gwack Y, Prakriya M, Srikanth S, Puppel S-H, Tanasa B, Hogan PG, Lewis RS, Daly M, Rao A. A mutation in Orai1 causes immune deficiency by abrogating CRAC channel function. Nature. 2006; 441:179–185. [PubMed: 16582901]
7. Vig M, Peinelt C, Beck A, Koomoa DL, Rabah D, Koblan-Huberson M, Kraft S, Turner H, Fleig A, Penner R, Kinet J-P. CRACM1 is a plasma membrane protein essential for store-operated Ca^{2+} entry. Science. 2006; 312:1220–1223. [PubMed: 16645049]
8. Zhang SL, Yeromin AV, Zhang XH-F, Yu Y, Safrina O, Penna A, Roos J, Stauderman KA, Cahalan MD. Genome-wide RNAi screen of Ca^{2+} influx identifies genes that regulate Ca^{2+} release-activated Ca^{2+} channel activity. Proc Natl Acad Sci U S A. 2006; 103:9357–9362. [PubMed: 16751269]
9. Calloway N, Vig M, Kinet J-P, Holowka D, Baird B. Molecular clustering of STIM1 with Orai1/CRACM1 at the plasma membrane depends dynamically on depletion of Ca^{2+} stores and on electrostatic interactions. Mol Biol Cell. 2009; 20:389–399. [PubMed: 18987344]

10. Barr VA, Bernot KM, Srikanth S, Gwack Y, Balagopalan L, Regan CK, Helman DJ, Sommers CL, Oh-Hora M, Rao A, Samelson LE. Dynamic movement of the calcium sensor STIM1 and the calcium channel Orai1 in activated T-cells: Puncta and distal caps. Mol Biol Cell. 2008; 19:2802–2817. [PubMed: 18448669]
11. Muik M, Frischauf I, Derler I, Fahrner M, Bergsmann J, Eder P, Schindl R, Hesch C, Polzinger B, Fritsch R, Kahr H, et al. Dynamic coupling of the putative coiled-coil domain of ORAI1 with STIM1 mediates ORAI1 channel activation. J Biol Chem. 2008; 283:8014–8022. [PubMed: 18187424]
12. Derler I, Madl J, Schütz G, Romanin C. Structure, regulation and biophysics of I_{CRAC}, STIM/Orai1. Adv Exp Med Biol. 2012; 740:383–410. [PubMed: 22453951]
13. Hou X, Pedi L, Diver MM, Long SB. Crystal structure of the calcium release– activated calcium channel Orai. Science. 2012; 338:1308–1313. [PubMed: 23180775]
14. Park CY, Hoover PJ, Mullins FM, Bachhawat P, Covington ED, Raunser S, Walz T, Garcia KC, Dolmetsch RE, Lewis RS. STIM1 clusters and activates CRAC channels via direct binding of a cytosolic domain to Orai1. Cell. 2009; 136:876–890. [PubMed: 19249086]
15. Derler I, Plenk P, Fahrner M, Muik M, Jardin I, Schindl R, Gruber HJ, Groschner K, Romanin C. The extended transmembrane Orai1 N-terminal (ETON) region combines binding interface and gate for Orai1 activation by STIM1. J Biol Chem. 2013; 288:29025–29034. [PubMed: 23943619]
16. Rothberg BS, Wang Y, Gill DL. Orai channel pore properties and gating by STIM: Implications from the Orai crystal structure. Sci Signal. 2013; 6:pe9. [PubMed: 23512988]
17. Feske S, Prakriya M, Rao A, Lewis RS. A severe defect in CRAC Ca^{2+} channel activation and altered K^+ channel gating in T cells from immunodeficient patients. J Exp Med. 2005; 202:651–662. [PubMed: 16147976]
18. Derler I, Fahrner M, Carugo O, Muik M, Bergsmann J, Schindl R, Frischauf I, Eshaghi S, Romanin C. Increased hydrophobicity at the N terminus/membrane interface impairs gating of the severe combined immunodeficiency-related ORAI1 mutant. J Biol Chem. 2009; 284:15903–15915. [PubMed: 19366689]
19. Derler I, Schindl R, Fritsch R, Romanin C. Gating and permeation of Orai channels. Front Biosci (Landmark Ed). 2012; 17:1304–1322. [PubMed: 22201805]
20. Hogan PG, Rao A. Store-operated calcium entry: Mechanisms and modulation. Biochem Biophys Res Commun. 2015; 460:40–49. [PubMed: 25998732]
21. Srikanth S, Jew M, Kim K-D, Yee M-K, Abramson J, Gwack Y. Junctate is a Ca^{2+}-sensing structural component of Orai1 and stromal interaction molecule 1 (STIM1). Proc Natl Acad Sci U S A. 2012; 109:8682–8687. [PubMed: 22586105]
22. Palty R, Raveh A, Kaminsky I, Meller R, Reuveny E. SARAF inactivates the store operated calcium entry machinery to prevent excess calcium refilling. Cell. 2012; 149:425–438. [PubMed: 22464749]
23. Srikanth S, Gwack Y. Orai1, STIM1, and their associating partners. J Physiol. 2012; 590:4169–4177. [PubMed: 22586216]
24. Walsh CM, Chvanov M, Haynes LP, Petersen OH, Tepikin AV, Burgoyne RD. Role of phosphoinositides in STIM1 dynamics and store-operated calcium entry. Biochem J. 2010; 425:159–168.
25. Calloway N, Owens T, Corwith K, Rodgers W, Holowka D, Baird B. Stimulated association of STIM1 and Orai1 is regulated by the balance of $PtdIns(4,5)P_2$ between distinct membrane pools. J Cell Sci. 2011; 124:2602–2610. [PubMed: 21750194]
26. Cao X, Choi S, Maléth JJ, Park S, Ahuja M, Muallem S. The ER/PM microdomain, PI(4,5)P2 and the regulation of STIM1-Orai1 channel function. Cell Calcium. 2015; 58:342–348. [PubMed: 25843208]
27. Abu-Arish A, Pandzic E, Goepp J, Matthes E, Hanrahan JW, Wiseman PW. Cholesterol modulates CFTR confinement in the plasma membrane of primary epithelial cells. Biophys J. 2015; 109:85–94. [PubMed: 26153705]
28. Gimpl G, Gehrig-Burger K. Cholesterol reporter molecules. Biosci Rep. 2007; 27:335–358. [PubMed: 17668316]

29. Dar O, Pecht I. Fcε receptor mediated Ca^{2+} influx into mast cells is modulated by the concentration of cytosolic free Ca^{2+} ions. FEBS Lett. 1992; 310:123–128. [PubMed: 1397260]
30. Kovarova M, Wassif CA, Odom S, Liao K, Porter FD, Rivera J. Cholesterol deficiency in a mouse model of Smith-Lemli-Opitz syndrome reveals increased mast cell responsiveness. J Exp Med. 2006; 203:1161–1171. [PubMed: 16618793]
31. Epand RM. Proteins and cholesterol-rich domains. Biochim Biophys Acta. 2008; 1778:1576–1582. [PubMed: 18423371]
32. Zhou Y, Meraner P, Kwon HT, Machnes D, Oh-hora M, Zimmer J, Huang Y, Stura A, Rao A, Hogan PG. STIM1 gates the store-operated calcium channel ORAI1 in vitro. Nat Struct Mol Biol. 2010; 17:112–116. [PubMed: 20037597]
33. Liu Y, Zheng X, Mueller GA, Sobhany M, DeRose EF, Zhang Y, London RE, Birnbaumer L. Crystal structure of calmodulin binding domain of Orai1 in complex with Ca^{2+}•calmodulin displays a unique binding mode. J Biol Chem. 2012; 287:43030–43041. [PubMed: 23109337]
34. Mullins FM, Park CY, Dolmetsch RE, Lewis RS. STIM1 and calmodulin interact with Orai1 to induce Ca^{2+}-dependent inactivation of CRAC channels. Proc Natl Acad Sci U S A. 2009; 106:15495–15500. [PubMed: 19706428]
35. Srikanth S, Jung H-J, Kim K-D, Souda P, Whitelegge J, Gwack Y. A novel EF-hand protein, CRACR2A, is a cytosolic Ca^{2+} sensor that stabilizes CRAC channels in T cells. Nat Cell Biol. 2010; 12:436–446. [PubMed: 20418871]
36. Li H, Papadopoulos V. Peripheral-type benzodiazepine receptor function in cholesterol transport. Identification of a putative cholesterol recognition/interaction amino acid sequence and consensus pattern. Endocrinology. 1998; 139:4991–4997.
37. Muik M, Fahrner M, Derler I, Schindl R, Bergsmann J, Frischauf I, Groschner K, Romanin C. A cytosolic homomerization and a modulatory domain within STIM1 C terminus determine coupling to ORAI1 channels. J Biol Chem. 2009; 284:8421–8426. [PubMed: 19189966]
38. Klein U, Gimpl G, Fahrenholz F. Alteration of the myometrial plasma membrane cholesterol content with β-cyclodextrin modulates the binding affinity of the oxytocin receptor. Biochemistry. 1995; 34:13784–13793. [PubMed: 7577971]
39. Raghuraman H, Chattopadhyay A. Interaction of melittin with membrane cholesterol: A fluorescence approach. Biophys J. 2004; 87:2419–2432. [PubMed: 15454440]
40. Hölttä-Vuori M, Uronen R-L, Repakova J, Salonen E, Vattulainen I, Panula P, Li Z, Bittman R, Ikonen E. BODIPY-cholesterol: A new tool to visualize sterol trafficking in living cells and organisms. Traffic. 2008; 9:1839–1849. [PubMed: 18647169]
41. Liao Y, Plummer NW, George MD, Abramowitz J, Zhu MX, Birnbaumer L. A role for Orai in TRPC-mediated Ca^{2+} entry suggests that a TRPC:Orai complex may mediate store and receptor operated Ca^{2+} entry. Proc Natl Acad Sci U S A. 2009; 106:3202–3206. [PubMed: 19221033]
42. Dionisio N, Galán C, Jardín I, Salido GM, Rosado JA. Lipid rafts are essential for the regulation of SOCE by plasma membrane resident STIM1 in human platelets. Biochim Biophys Acta. 2011; 1813:431–437. [PubMed: 21255618]
43. Galan C, Woodard GE, Dionisio N, Salido GM, Rosado JA. Lipid rafts modulate the activation but not the maintenance of store-operated Ca^{2+} entry. Biochim Biophys Acta. 2010; 1803:1083–1093. [PubMed: 20600358]
44. Jardin I, Salido GM, Rosado JA. Role of lipid rafts in the interaction between hTRPC1, Orai1 and STIM1. Channels. 2008; 2:401–403. [PubMed: 18843204]
45. Chantôme A, Potier-Cartereau M, Clarysse L, Fromont G, Marionneau-Lambot S, Guéguinou M, Pagès J-C, Collin C, Oullier T, Girault A, Arbion F, et al. Pivotal role of the lipid Raft SK3–Orai1 complex in human cancer cell migration and bone metastases. Cancer Res. 2013; 73:4852–4861. [PubMed: 23774210]
46. Miller CM, Brown AC, Mittal J. Disorder in cholesterol-binding functionality of CRAC peptides: A molecular dynamics study. J Phys Chem B. 2014; 2014:13169–13174.
47. Li H, Yao Z-x, Degenhardt B, Teper G, Papadopoulos V. Cholesterol binding at the cholesterol recognition/ interaction amino acid consensus (CRAC) of the peripheral-type benzodiazepine receptor and inhibition of steroidogenesis by an HIV TAT-CRAC peptide. Proc Natl Acad Sci U S A. 2001; 98:1267–1272. [PubMed: 11158628]

48. Scolari S, Muller K, Bittman R, Herrmann A, Muller P. Interaction of mammalian seminal plasma protein PDC-109 with cholesterol: Implications for a putative CRAC domain. Biochemistry. 2010; 49:9027–9031. [PubMed: 20863067]
49. Rosenhouse-Dantsker A, Noskov S, Durdagi S, Logothetis DE, Levitan I. Identification of novel cholesterol-binding regions in Kir2 channels. J Biol Chem. 2013; 288:31154–31164. [PubMed: 24019518]
50. Picazo-Juárez G, Romero-Suárez S, Nieto-Posadas A, Llorente I, Jara-Oseguera A, Briggs M, McIntosh TJ, Simon SA, Ladrón-de-Guevara E, Islas LD, Rosenbaum T. Identification of a binding motif in the S5 helix that confers cholesterol sensitivity to the TRPV1 ion channel. J Biol Chem. 2011; 286:24966–24976. [PubMed: 21555515]
51. Kucerka N, Nieh MP, Pencer J, Sachs JN, Katsaras J. What determines the thickness of a biological membrane. Gen Physiol Biophys. 2009; 28:117–125. [PubMed: 19592708]
52. Nyholm TKM, van Duyl B, Rijkers DTS, Liskamp RMJ, Killian JA. Probing the lipid-protein interface using model transmembrane peptides with a covalently linked acyl chain. Biophys J. 2011; 101:1959–1967. [PubMed: 22004750]
53. Yuan C, O'Connell RJ, Jacob RF, Mason RP, Treistman SN. Regulation of the gating of BK_{Ca} channel by lipid bilayer thickness. J Biol Chem. 2007; 282:7276–7286. [PubMed: 17209047]
54. Tong J, Briggs MM, McIntosh TJ. Water permeability of aquaporin-4 channel depends on bilayer composition, thickness, and elasticity. Biophys J. 2012; 103:1899–1908. [PubMed: 23199918]
55. Kato N, Nakanishi M, Hirashima N. Cholesterol depletion inhibits store-operated calcium currents and exocytotic membrane fusion in RBL-2H3 cells. Biochemistry. 2003; 42:11808–11814. [PubMed: 14529292]
56. Mahammad S, Parmryd I. Cholesterol depletion using methyl-β-cyclodextrin. Methods Mol Biol. 2015; 1232:91–102. [PubMed: 25331130]
57. Grynkiewicz G, Poenie M, Tsien RY. A new generation of Ca2+ indicators with greatly improved fluorescence properties. J Biol Chem. 1985; 260:3440–3450. [PubMed: 3838314]
58. Singh A, Hamedinger D, Hoda J-C, Gebhart M, Koschak A, Romanin C, Striessnig J. C-terminal modulator controls Ca^{2+}-dependent gating of Ca_V 1.4 L-type Ca^{2+} channels. Nat Neurosci. 2006; 9:1108–1116. [PubMed: 16921373]
59. Derler I, Hofbauer M, Kahr H, Fritsch R, Muik M, Kepplinger K, Hack ME, Moritz S, Schindl R, Groschner K, Romanin C. Dynamic but not constitutive association of calmodulin with rat TRPV6 channels enables fine tuning of Ca^{2+}-dependent inactivation. J Physiol. 2006; 577:31–44. [PubMed: 16959851]
60. Xia Z, Liu Y. Reliable and global measurement of fluorescence resonance energy transfer using fluorescence microscopes. Biophys J. 2001; 81:2395–2402. [PubMed: 11566809]
61. Berney C, Danuser G. FRET or no FRET: A quantitative comparison. Biophys J. 2003; 84:3992–4010. [PubMed: 12770904]
62. Muik M, Fahrner M, Schindl R, Stathopulos P, Frischauf I, Derler I, Plenk P, Lackner B, Groschner K, Ikura M, Romanin C. STIM1 couples to ORAI1 via an intramolecular transition into an extended conformation. EMBO J. 2011; 30:1678–1689. [PubMed: 21427704]
63. Schindl R, Fritsch R, Jardin I, Frischauf I, Kahr H, Muik M, Riedl MC, Groschner K, Romanin C. Canonical transient receptor potential (TRPC) 1 acts as a negative regulator for vanilloid TRPV6-mediated Ca^{2+} influx. J Biol Chem. 2012; 287:35612–35620. [PubMed: 22932896]
64. Bisaillon JM, Motiani RK, Gonzalez-Cobos JC, Potier M, Halligan KE, Alzawahra WF, Barroso M, Singer HA, Jourd'heuil D, Trebak M. Essential role for STIM1/Orai1-mediated calcium influx in PDGF-induced smooth muscle migration. Am J Physiol Cell Physiol. 2010; 298:C993–C1005. [PubMed: 20107038]
65. Woodard GE, Salido GM, Rosado JA. Enhanced exocytotic-like insertion of Orai1 into the plasma membrane upon intracellular Ca^{2+} store depletion. Am J Physiol Cell Physiol. 2008; 294:C1323–C1331. [PubMed: 18400989]

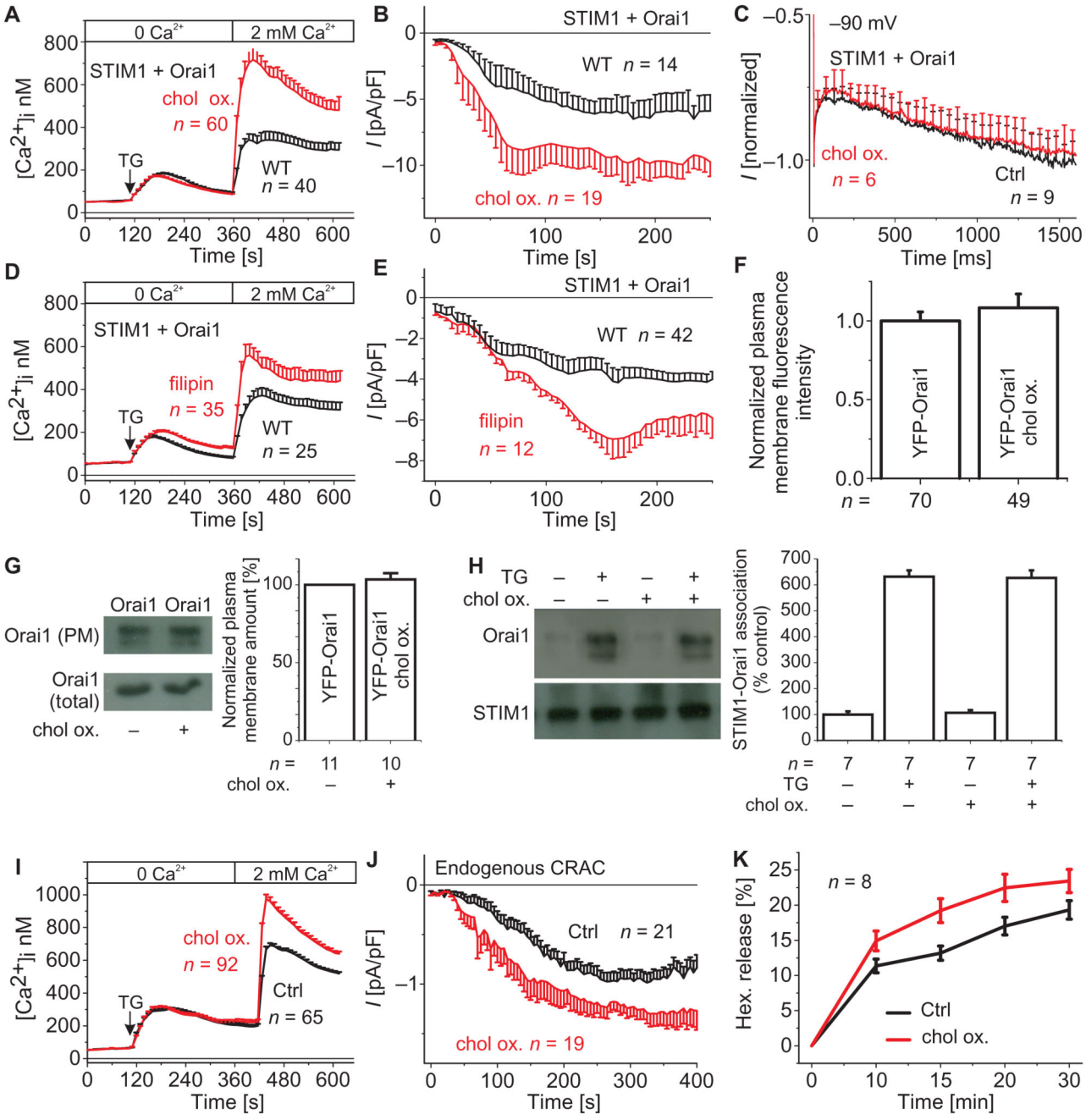

Fig. 1. Cholesterol depletion in STIM1- and Orai1-containing HEK293 cells and in RBL mast cells increases Ca^{2+} entry and endogenous CRAC currents, respectively, as well as mast cell degranulation in RBL cells.

(**A**) Changes in intracellular Ca^{2+} concentrations $[Ca^{2+}]_i$ in cholesterol oxidase (chol ox.)–treated HEK293 cells expressing STIM1 and Orai1 compared to untreated cells [wild type (WT)] expressing Orai1 and STIM1 (t = 400 s; $P < 0.05$, Student's t test). (**B**) Respective time courses for (A) whole-cell inward currents upon passive store depletion by EGTA at −74 mV of cholesterol oxidase–treated HEK293 cells expressing STIM1 and Orai1 compared to untreated cells expressing Orai1 and STIM1 (t= 150 s; P< 0.05, Student's t

test). (**C**) Mean inactivation profile at −90 mV of normalized current traces of HEK293 cells expressing STIM1 and Orai1 with and without incubation with cholesterol oxidase. Ctrl, control. (**D**) Changes in intracellular Ca^{2+} concentrations in filipin-treated HEK293 cells expressing STIM1 and Orai1 compared to untreated cells expressing Orai1 and STIM1 (t = 400 s; $P < 0.05$, Student's t test). (**E**) Time course of whole-cell inward currents upon passive store depletion by EGTA at −74 mV of filipin-treated HEK293 cells expressing STIM1 and Orai1 compared to untreated cells expressing Orai1 and STIM1 (t = 150 s; $P < 0.05$, Student's t test). For (A) to (E), n represents the number of tested cells. (**F**) Western blot and bar graph showing the amount of Orai1 with or without cholesterol oxidase. (**G**) Coimmunoprecipitation of STIM1 and Orai1 before and after cholesterol oxidase incubation. PM, plasma membrane. For (F) and (G), n represents the number of experiments. (**H**) Bar graph comparing the plasma membrane intensities of control and cholesterol oxidase–treated cells. n represents the number of tested cells taken from three to five transfections. (**I**) Changes in intracellular Ca^{2+} concentrations upon application of TG and ensuing perfusion with a Ca^{2+}-containing solution in RBL cells upon incubation with cholesterol oxidase (t = 480 s; $P < 0.05$, Student's t test). (**J**) Time course of whole-cell currents upon passive store depletion with EGTA at −74 mV of RBL cells upon incubation with cholesterol oxidase compared to control cells (t = 300 s; $P < 0.05$, Student's t test). For (A) and (B), n represents the number of tested cells. (**K**) Hexosaminidase release (hex. release) of RBL cells without and with incubation with cholesterol oxidase ($P < 0.05$). n represents the number of independent experiments.

Europe PMC Funders Author Manuscripts

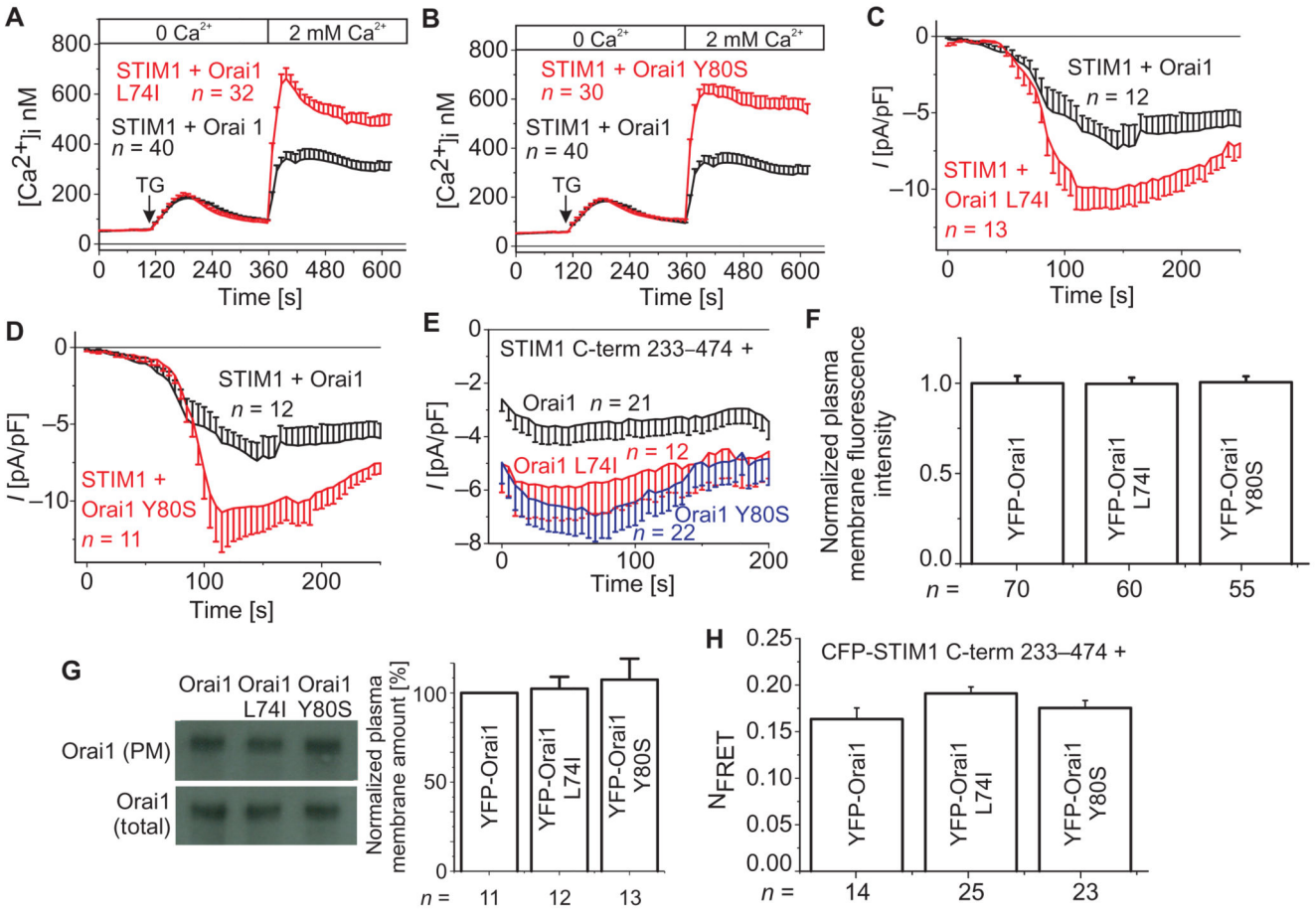

Fig. 2. Mutations within the CB motif in Orai1 lead to significantly enhanced Ca^{2+} entry and current density.

(**A** and **C**) Changes in intracellular Ca^{2+} concentrations upon TG application and perfusion with a Ca^{2+}-containing solution in HEK293 cells expressing STIM1 with (A) Orai1 L74I or (C) Orai1 Y80S, compared to WT Orai1–expressing cells ($t = 400$ s; $P < 0.05$, Student's t test). (**B** and **D**) Time course of whole-cell currents upon passive store depletion by EGTA at −74 mV of HEK293 cells expressing STIM1 and (B) Orai1 L74I or (D) Orai1 Y80S, compared to cells expressing WT Orai1 ($t = 150$ s; $P < 0.05$, Student's t test). (**E**) Time course of whole-cell currents of cells expressing STIM1 C-terminal fragment encompassing amino acids 233–474 (C-term 233–474) with CB motif Orai1 mutants or WT Orai1. For (A) to (E), n represents the number of cells. (**F**) Western blot and bar graph showing the amounts of Orai1, Orai1 L74I, and Orai1 Y80S in the plasma membrane. n represents the number of experiments. (**G**) Bar graph comparing the plasma membrane intensities of control and CB motif mutant–containing cells. n represents the number of test cells from three to five transfections. (**H**) Bar graph depicting the FRET intensities of STIM1 C-term 233–474 with Orai1, Orai1 L74I, and Orai1 Y80S. n represents the number of cells.

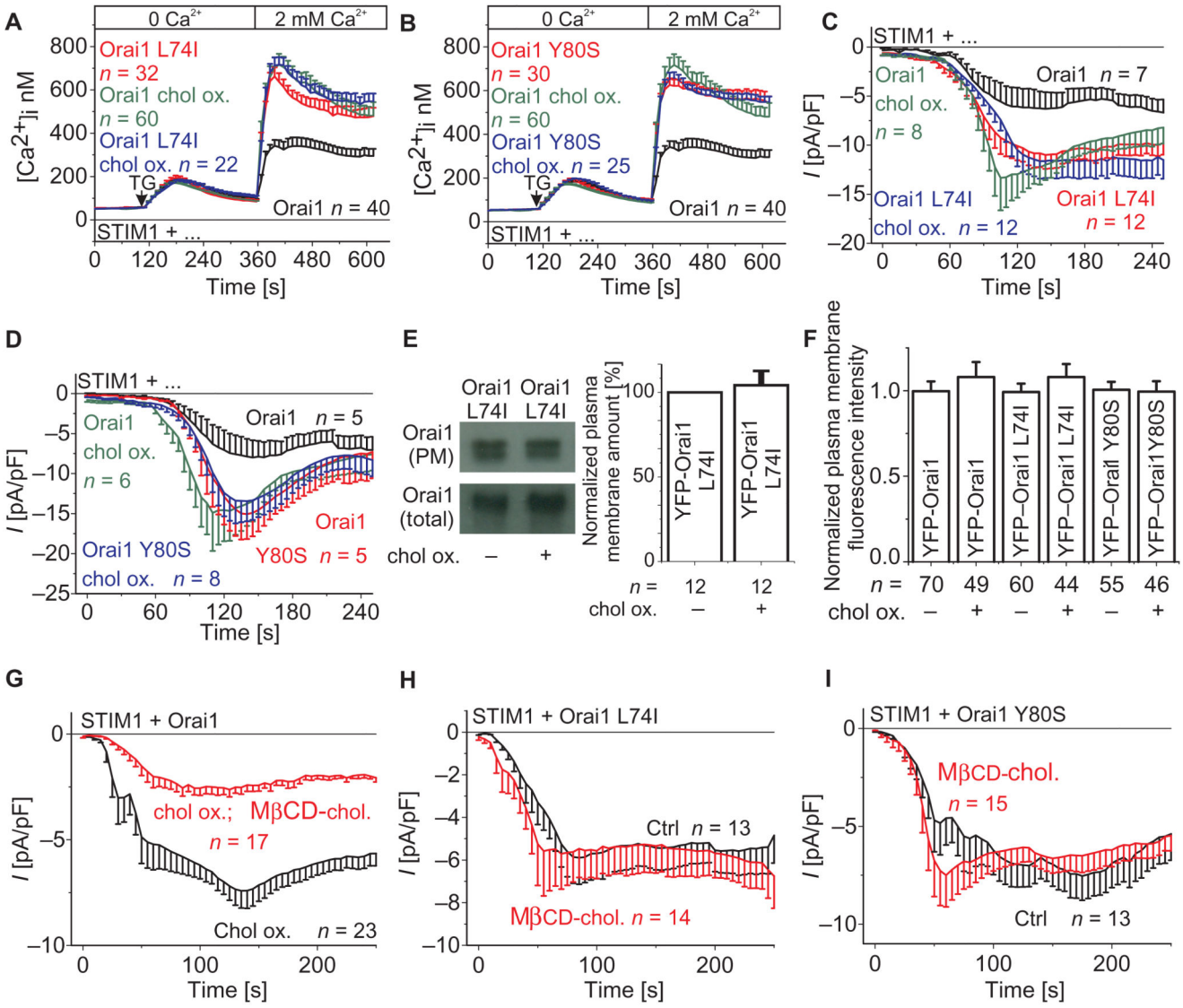

Fig. 3. Orai1 CB motif mutants are not affected by cholesterol depletion or replenishment, and reloading of cholesterol reverses the effect of cholesterol oxidase on WT Orai1.

(**A** and **B**) Changes in intracellular Ca^{2+} concentrations in HEK293 cells expressing STIM1 with (A) Orai1 L74I or (B) Orai1 Y80S compared to WT Orai1. Both WT and CB motif mutants were analyzed in untreated and/or cholesterol oxidase–treated cells. (**C** and **D**) Time course of whole-cell currents upon passive store depletion by EGTA at −74 mV of HEK293 cells expressing STIM1 and (C) Orai1 L74I or (D) Orai1 Y80S, compared to untreated, treated, or cholesterol-preincubated cells expressing WT Orai1 and or the single point mutants. For (A) to (D), *n* represents the number of tested cells. (**E**) Western blot and bar graph comparing the amount of Orai1 L74I in the plasma membrane before and after incubation with cholesterol oxidase. *n* represents the number of experiments. (**F**) Bar graph comparing the plasma membrane intensities of control and CB motif mutant expressing cells in the absence and presence of cholesterol oxidase. *n* represents the number of tested cells, which have been taken from three to five transfections. (**G**) Time course of whole-cell

currents upon passive store depletion by EGTA at −74 mV of HEK293 cells expressing STIM1 and Orai1 that were incubated with cholesterol oxidase compared to those preincubated with MβCD-cholesterol before cholesterol oxidase treatment (t = 150 s; P < 0.001, Student's t test). (**H** and **I**) Time course of whole-cell currents upon passive store depletion by EGTA at −74 mV of HEK293 cells expressing STIM1 and Orai1 L74I (H) or Orai1 Y80S (I) without and with incubation with MβCD-cholesterol. For (G) to (I), n represents the number of tested cells.

Europe PMC Funders Author Manuscripts

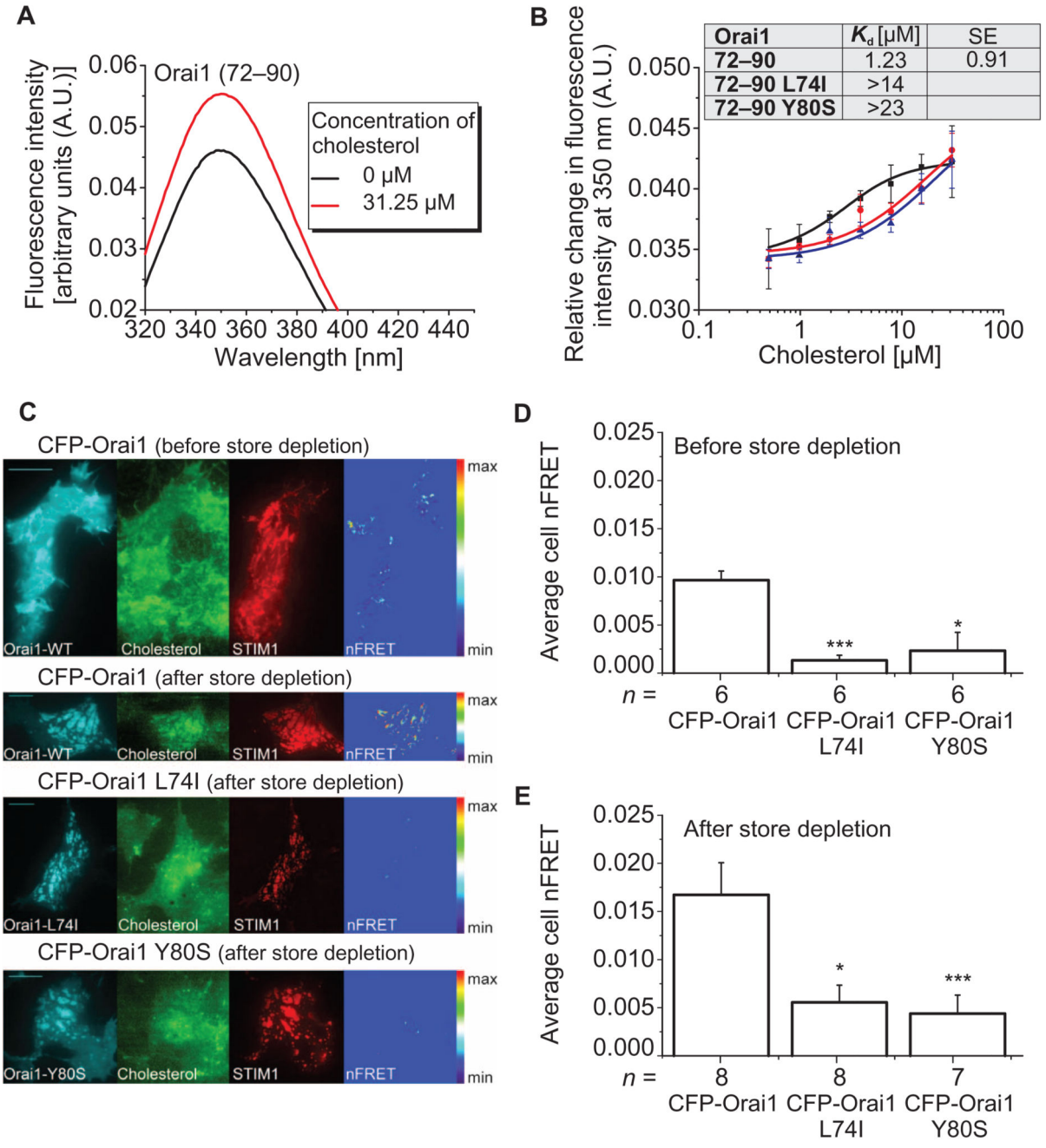

Fig. 4. Mutant Orai1 N-terminal peptides and full-length Orai1 mutant channels display reduced association with cholesterol compared to WT peptides and Orai1.

(**A**) Intensity profile of Orai1 (72–90) N-terminal peptide in the absence and presence of cholesterol. The figure is representative of three independent experiments. (**B**) Binding curves displaying changes in the intrinsic fluorescence of Orai1 (72–90), Orai1 (72–90) L74I, and Orai1 (72–90) Y80S with increasing cholesterol concentrations. Inset shows the apparent K_d of the WT peptide compared to the mutants. Each binding curve for the WT and mutant peptides is derived from the average of $n = 3$ independent experiments. Error bars are

SDs. Excitation wavelength was 280 nm in (A) and (B). (**C**) FRET-TIRF microscopy of HEK293 cells before and after store depletion. Cells were transfected with the indicated Orai construct and mCherry-STIM1 (STIM1) and loaded with TopFluor Cholesterol (Cholesterol). Images on the right (nFRET) show FRET-positive pixels after correction for bleedthrough and non-colocalization. (**D** and **E**) Average nFRET of cells expressing the indicated Orai construct before and after (E) store depletion. Statistical analysis was performed with *t* test (control: CFP-Orai1, $^{**}P < 0.05$ and $^{***}P < 0.005$). *n* represents the number of tested cells, which have been taken from three to five transfections. Scale bars, 10 μm.

Europe PMC Funders Author Manuscripts